J Mater Sci (2010) 45:5844–5850
DOI 10.1007/s10853-010-4660-8

Production of Ti–13Nb–13Zr alloy for surgical implants by powder metallurgy

V. A. R. Henriques · E. T. Galvani · S. L. G. Petroni · M. S. M. Paula · T. G. Lemos

Received: 30 October 2009 / Accepted: 26 May 2010 / Published online: 12 June 2010

Abstract The Ti–13Nb–13Zr near-β alloy was developed aiming the replacement of the traditional Ti–6Al–4V alloy in surgical implants owing to its larger biocompatibility. Samples of this alloy were obtained using the blended elemental technique from hydrided powders. The isochronal sintering of the compacts for 2 h was carried out in the range 900–1,400 °C with a heating rate of 20 °C min^{-1}. In this work, the behavior of the elementary powders during sintering and the corresponding microstructural evolution were investigated. The alloy was characterized by means of scanning electron microscopy (SEM) in the backscattered mode, X-ray diffraction, and density measurements. The results indicate that the homogenization of the alloy is diffusion-controlled. With increasing temperature, homogenization of the alloy takes place and a fine plate-like $\alpha + \beta$ structure is found throughout the microstructure in temperatures above 1,300 °C. The process variables were defined aiming to minimize interstitial pick-up (C, O, and N) and avoiding intensive grain growth.

V. A. R. Henriques (✉) · S. L. G. Petroni
AMR, Divisão de Materiais, Instituto de Aeronáutica e Espaço (IAE), Centro Técnico Aeroespacial (CTA), São José dos Campos, SP 12228-904, Brazil
e-mail: vinicius@iae.cta.br

S. L. G. Petroni
e-mail: slpetroni@iae.cta.br

E. T. Galvani · M. S. M. Paula
ITA, Instituto Tecnológico de Aeronáutica, Centro Técnico Aeroespacial (CTA), São José dos Campos, SP 12228-904, Brazil
e-mail: eduardotgalvani@yahoo.com.br

M. S. M. Paula
e-mail: matheus@gmx.com

T. G. Lemos
EEL, Escola de Engenharia de Lorena, Lorena, SP, Brazil
e-mail: tgorla@hotmail.com

Introduction

Titanium and its alloys have become one of the most attractive classes of biomedical implant materials. They are generally preferred to stainless steels and Co–Cr alloys because of their low density, superior biocompatibility and corrosion resistance, good mechanical properties, and low-elastic modulus [1–3].

The first generation orthopedic $\alpha + \beta$ titanium alloys such as Ti–6Al–4V ELI (extra low interstitial), Ti–6Al–7Nb and Ti–5Al–2.5Fe are already in use. In recent years, second generation low-modulus near β and β type titanium alloys have been developed for orthopedic applications in order to avoid the "stress shielding" effect caused by the modulus mismatch between the implant and the bone [4–6].

Ti–13Nb–13Zr is a near β alloy formulated at the beginning of the 1990s to be used in orthopedic applications due to its low Young's modulus (40–80 GPa) and its non-toxic composition. It presents tensile values of approximately 1,300 MPa and a superior corrosion resistance when compared to Ti–6Al–4V and Ti–6Al–7Nb alloys [7–10].

Ti–13Nb–13Zr has niobium as a beta-phase stabilizer. The other alloying element, zirconium, is isomorphous with both the alpha and beta phases of titanium. A combination of these two alloying elements has made it possible to develop a structure that is a "near" beta phase supposedly possessing a superior corrosion resistance over the alpha–beta phase alloys, with enough alpha phase present in the final structure to provide the necessary

mechanical strength. It has been proposed that Ti–13Nb–13Zr alloy is more favorable for orthopedic implants than Ti–6Al–4V alloy because of its superior corrosion resistance and biocompatibility [11–13].

Reasons for this superiority have included the fact that less metal ion release is likely to occur during spontaneous passivation of Ti–13Nb–13Zr alloy because the corrosion products of the minor alloying elements, niobium and zirconium, are less soluble than those of aluminum and vanadium. Also, that the passive oxide layer on the surface of the alloy is more inert consisting of a dense rutile structure providing greater protection to the underlying alloy [14–17].

The machining cost of titanium alloys is very high. The powder metallurgy (P/M) process is a near-net-shape process, and therefore, effective in the reduction of the machining cost of titanium alloys [18]. The P/M process is also advantageous to fabricate alloys, which are difficult to fabricate through the ingot melting (IM) process. The possibility of hot isostatic pressing or forging applied after sintering reduces the residual porosity. Metal injection molding (MIM) is also applicable to fabricate titanium alloys for biomedical applications [19]. Recent low-modulus titanium alloys for biomedical applications (such as Ti–13Nb–13Zr and Ti–35Nb–7Zr–5Ta) contain a large amount of alloying elements with much higher melting temperatures and density, such as Nb and Ta compared with Ti. In these cases, the P/M process is also advantageous to make homogeneous alloys [20–23]. The mechanical properties of Ti–29Nb–13Ta–4.6Zr fabricated through the IM process and P/M process are equivalent to those of Ti–29Nb–13Ta–4.6Zr, although 0.2% proof stress is lower in PM alloys than in IM alloys [2]. Reactive plasma spraying (RPS) from titanium powders for protective coatings have been used in industrial area in recent years [24].

The blended elemental (BE) approach is potentially the lowest cost titanium P/M process available. Unfortunately, parts are limited in size and complexity, as well as less than 100% of theoretical density, which would adversely affect mechanical properties. Recent developments, such as using hydrided powders, have enabled the fabrication of BE parts to over 99% of full density, resulting in significantly improved properties. Further studies and developments show that this approach may be well suited to reduce the cost of producing industrial parts making titanium more cost competitive with other materials commonly used in many applications [25–28].

A significant influence on mechanical behavior of commercial pure (CP) titanium is brought about by hydrogen, nitrogen, carbon, and oxygen, which dissolves interstitially in titanium and have a potent effect on mechanical properties. These effects are carried over to titanium alloys in varying degrees [29]. Interstitial elements are those elements that are significantly smaller than the titanium atom and can be dissolved in the titanium crystal lattice as solid solutions without substituting the titanium atom sites [30].

The aim of this article is to investigate the microstructural evolution and the behavior of the hydrided powders during sintering in order to determine the influence of the key process variables on the microstructure of this alloy for an efficient and safe application in surgical implants.

Experimental

The BE method followed by a sequence of uniaxial and cold isostatic pressing with subsequent densification by sintering was used for the preparation of the Ti–13Nb–13Zr samples.

Titanium and zirconium powders were obtained by hydriding treatment from sponge fines. Hydriding was carried out at 500 °C, in a vacuum furnace, for 3 h, under a positive pressure. After cooling to room temperature, the friable hydride was milled in a titanium container, in vacuum condition (10^{-3} Torr) for 6 h. Nb powder was obtained using the same route, however, using machining chips and hydriding temperatures significantly higher (800 °C). Table 1 shows the principal characteristics, and Table 2 presents the interstitial contents of these powders.

The starting powders were weighed in batches of about 100 g, dried for 1 h in stove and blended for 60 min in a planetary mill with six drips of alcohol. After blending,

Table 1 Characteristics of the powders used in the Ti–13Nb–13Zr alloy preparation

Characteristic	Ti	Nb	Zr
Melting point (°C)	1670	2468	1850
Mean particles size (μm)	7.30	4.90	2.57
Particle morphology	Angular	Angular	Angular
Density	4.51	8.58	6.40
Melting point (°C)	1670	2468	1850
Production process	Hydriding	Hydriding	Hydriding

Table 2 Interstitial contents of the hydrided powders used in this investigation

Hydrided powder	Impurity content (wt%)		
	O	N	C
Ti	0.670	0.500	0.030
Nb	0.450	0.046	0.018
Zr	1.090	0.300	0.022

powders were cold uniaxially pressed at 80 MPa, in cylindrical 15 mm diameter steel die without lubricants. Afterward, the green compacts were encapsulated under vacuum in flexible latex molds and cold isostatically pressed at 350 MPa during 30 s aiming to increase their green density.

Sintering was carried out in niobium crucible, under high vacuum condition (10^{-7} Torr), using a Thermal Technology Inc. model Astro 1000 equipment. Sintering temperatures ranged between 900 and 1,400 °C with a heating rate equal to 20 °C/min. After reaching the nominal temperature, samples were hold at the chosen temperature for 2 h and then furnace-cooled to room temperature. Metallographic preparation was carried out using conventional techniques. Specimens were etched with a Kroll solution: (3 mL HF:6 mL HNO_3:100 mL H_2O) to reveal its microstructure. The micrographs were obtained using a scanning electron microscope (SEM) LEO model 435 Vpi, in the backscattered mode (BSE) to stress composition contrast. X-ray diffraction (XRD) was performed using Cu-Kα radiation at 30 kV (Rich-Seifert). Sintered densities were determined by water immersion method. The chemical composition of the sintered samples was determined by atomic emission plasma spectrometry with an ICP (Inductively Coupled Plasma) equipment, using ASTM E2371-04 pattern. Chemical composition of the constituent phases in terms of Ti, Nb, and Zr was determined using standardless semi-quantitative EDS analyses in the SEM. Oxygen and nitrogen were determined by the inert gas fusion technique using a LECO TC500 equipment. Carbon was determined by combustion-infrared spectrophotometry. Sampling for chemical analyses was performed in the central region of the sintered compacts. Microhardness measurements were carried out in a Micromet 2004 equipment, Buehler, with load of 0.2 kgf. The expansion/contraction behavior of a Ti–13Nb–13Zr compact during sintering was examined by a dilatometer, where a green compact with a 6 mm diameter and a 15 mm length was heated in the same sintering conditions at 1,400 °C, using hydrided and dehydrided powders. Classical 4 point flexion test were performed in samples sintered at 1,400 °C in order to estimate the mechanical properties.

Results and discussion

Densification and microstructural evolution

The samples presented high densification, varying between 69 and 71% of the theoretical density, after cold isostatic pressing and, between 93 and 97%, after sintering at 1,400 °C, with homogeneous microstructure.

In order to quantify the influence of sintering temperature on densification of the BE–Ti–13Nb–13Zr samples, the isochronal sintering was performed, with holding time of 2 h (Fig. 1). Density varies not very much from 900 up to 1,100 °C. Densification is faster between 1,100 and 1,400 °C, in the β-phase range with accompanying increase in diffusivity, reaching a maximum value of about 97% of theoretical density.

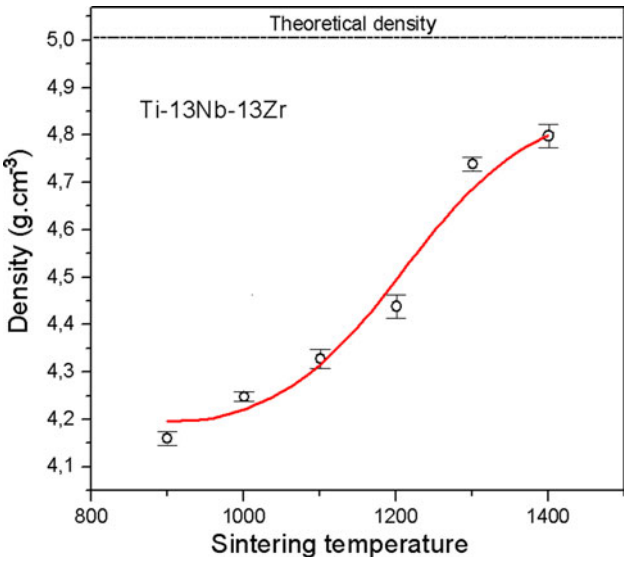

Fig. 1 Plot of density vs. sintering temperature for BE–Ti–13Nb–13Zr samples (900–1,400 °C, heating rate equal to 20 °C min^{-1}). Holding time at nominal temperature was 2 h. *Dotted line* indicates the theoretical density of the alloy

The microstructural analysis shows that a Widmanstätten-like microstructure grows with the dissolution of the niobium particles from increasing of the sintering temperature.

Figure 2 presents the microstructural evolution of the samples after sintering with nominal composition BE–/Ti–13Nb–13Zr from 900 to 1,400 °C. Concerning the alloy microstructure, the gray scale areas are α-phase plates. The β-phase, present among the α-phase areas, gives rise to a white contrast. Black areas are pore.

For specimens sintered at 900 °C, the microstructure consists of angular titanium particles (gray contrast) resembling their original morphology and niobium particles (brighter ones). Similar behavior has been also observed during heating of BE–Ti–6Al–7Nb compacts [19]. The dissolution of niobium particles becomes evident. The former angular-shaped niobium particles become rounded and their size decreased with time. The boundaries between the angular Ti and Nb particles become diffuse. The dissolution of zirconium particles in both α and β areas is fast with the temperature increase (being completely dissolved in temperatures above 1,000 °C). Furthermore, the first two-phase areas resembling a Widmanstätten structure become distinguishable. These areas consist of a pure niobium core (a strong β-stabilizer in titanium alloys)

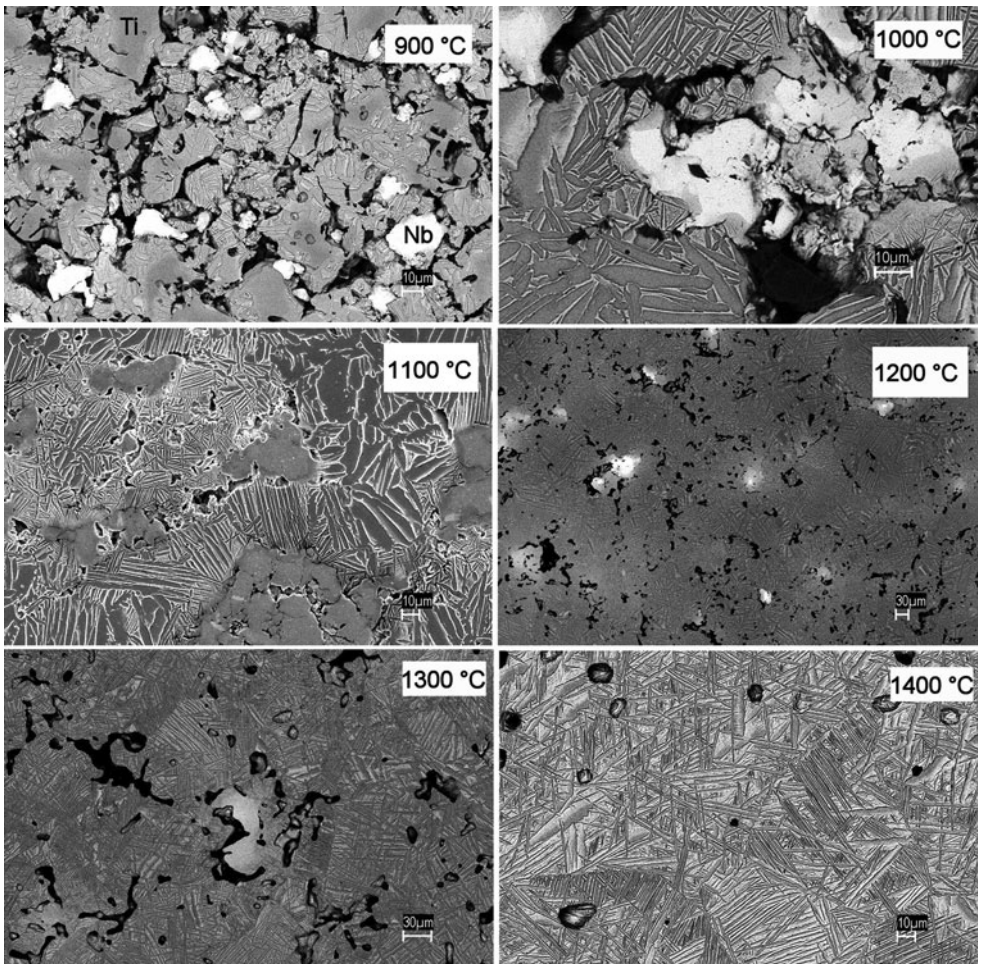

Fig. 2 Microstructural evolution of the BE–Ti–13Nb–13Zr during sintering. All samples were sintered at the nominal temperature for 2 h and heating rate equal to 20 °C min^{-1}

surrounded by a two-phase microstructure. With increasing sintering temperature, the dissolution of the niobium particles continues with consequent increase in the volume fraction of the two-phase structure.

The dissolution of niobium particles is very fast and at 1,000 °C, there are few regions without a two-phase microstructure. In the temperature range 1,000–1,300 °C, the most noticeable microstructural features are the spreading of the $\alpha + \beta$ structure and the chemical homogenization of the alloy. At 1,300 °C, the larger niobium particles present in the initial powder size distribution are found almost dissolved in the core of the Widmanstätten-like structure, whereas the finer ones have vanished in the microstructure. The specimens of the Ti–13Nb–13Zr alloy sintered at high temperatures (≥1,400 °C) display a fine plate-like alpha plus beta structure with alpha on grain boundary. Individual niobium areas are found completely dissolved. A few remaining pores are still found and density above 90% is observed. From 1,400 °C, a homogeneous microstructure is obtained and the chemical composition is reasonably homogeneous throughout the microstructure (at SEM resolution level). It does not exclude the possibility of very fine particles in the nanometer-range coexist in the microstructure. The samples presented hardness values around 300 HV, near the observed in samples produced by the conventional methods (melting and forging) [8].

A typical issue related to the hydrided powders flow is observed in the microstructural evolution. The hydrided powders present an angular and irregular morphology, which increases the surface area. Thus, the attrition between the particles increases, providing low flow and low compression rates. Figure 3 presents areas with agglomerations of niobium particles that take place due to the low-powder flow, preventing a good homogenization among the elemental hydrided particles, what demand high-sintering temperatures to the total dissolution of these agglomerates and complete homogenization of the alloy. These Nb agglomerated area is a problem directly related with the residual porosity.

Chemical composition of BE–Ti–13Nb–13Zr alloys

Results of ICP analyses reveal no appreciable changes in terms of Ti, Zr, and Nb contents during sintering of this

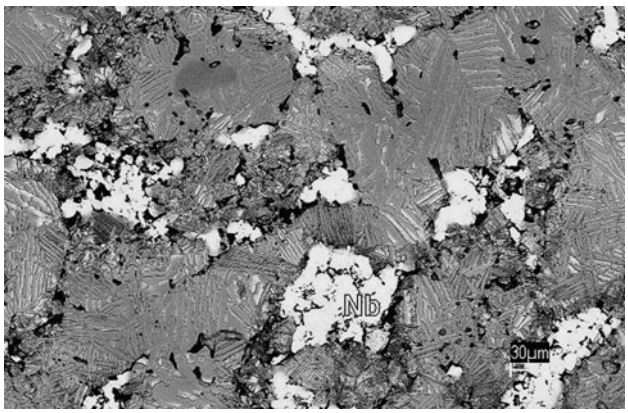

Fig. 3 Microstructure of Ti–13Nb–13Zr sample sintered at 1,100 °C presenting areas with niobium particle agglomerations

alloy. The nominal composition was kept nearly unchanged even in specimens sintered at 1,400 °C for 2 h. An advantage of P/M lies on the efficiency of the chemical composition control. A slight decrease in the final Zr content was observed lying close to 12.8 wt% (12.5–14% is the range specified in ASTM F1713).

Concerning interstitial impurities, results shown in Table 3 reveal the occurrence of a significant pick-up during P/M processing of this alloy, in terms of O absorption, reaching 1.32 wt% after sintering at 1,400 °C. Since the sintering was carried out under high vacuum condition (10^{-7} Torr), this pick-up is related to the oxygen absorption during the stages of the alloy processing by P/M, especially the hydriding stage (including milling) and the blending stage (with planetary milling) due to the heating in a not very protective atmosphere. The identification of these O levels and the optimization of the process based in the reduction of the interstitial contents will be targets of a future work.

Figure 4 shows the importance of the niobium particles in the β-phase stabilization and the spreading of the Widmanstätten structure. The β plates formation starting from the niobium agglomerates and its contribution for the sample densification is perfectly observed in Fig. 4a. Details of the particles diffusion are seen in Fig. 4b. The composition profile shows that the Zr content remains very low, whereas Nb concentration varies along the test line, being richer in the core of the left side regions (areas rich in Nb). Concentration of niobium decreases along the test line

Table 3 Chemical composition of Ti–13Nb–13Zr sintered at 1,400 °C

Condition (°C/2 h)	Impurity content (wt%)		
	O	N	C
1400	1.290	0.031	0.070

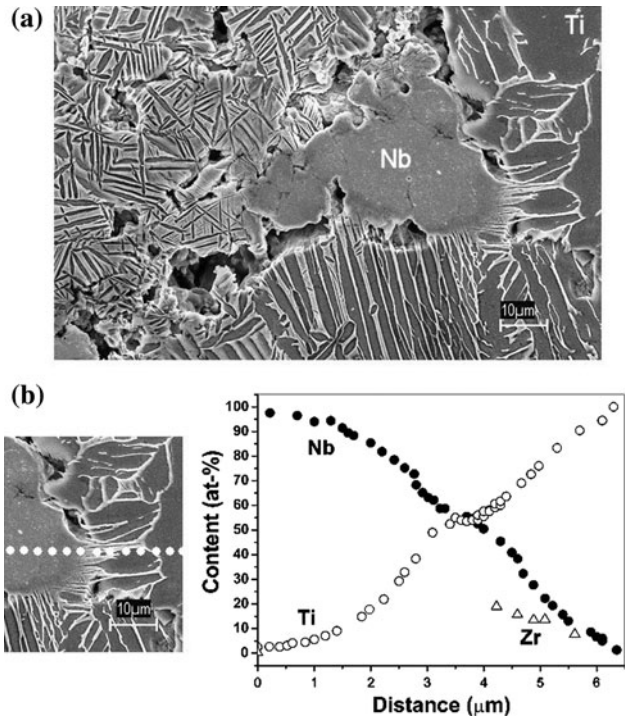

Fig. 4 **a** Dissolution of niobium agglomerates and beginning of a Widmanstätten-like microstructure. **b** Line scan (*dotted line*) showing the variation of Ti, Nb, and Zr contents at the contact point of distinct areas predominantly with Nb and Ti

as in direction of the right side (areas rich in Ti). It can be observed that the presence of small amounts of zirconium preferentially dissolved in $\alpha + \beta$ areas recently formed around the Nb area.

Results of EDS analyses performed in the plate-like α and intergranular β microstructure found in specimens sintered at 1,400 °C for 2 h indicate a composition of the α-phase close to 75.28%Ti–15.03%Nb–9.69%Zr (in wt%), whereas, the β-phase consists of 62.65%Ti–22.09%Nb–15.26%Zr (in wt%). The EDS analyses in the β-phase were performed in regions larger than 1 μm in width to avoid matrix interference. The volume fraction of β phase measured in this alloy is about 10%. The EDS results indicate superior niobium content in β-phase, due to its power of preferential stabilization of this phase. Zirconium is capable of stabilizing both α- and β-phase titanium alloy, but act by being in solution in the alloy as a β-stabilizer alloy (15.26% in β-phase). It is further believed that the larger ionic radius of zirconium (35% larger than that of titanium) helps to disrupt ionic bonding forces in the alloy resulting in some reduction in the modulus of elasticity [8].

X-ray diffraction analysis was carried out in the sintering temperature range between 900 and 1,400 °C. These analysis revealed only peaks of niobium and α and β titanium phases, not being identified peaks related to the

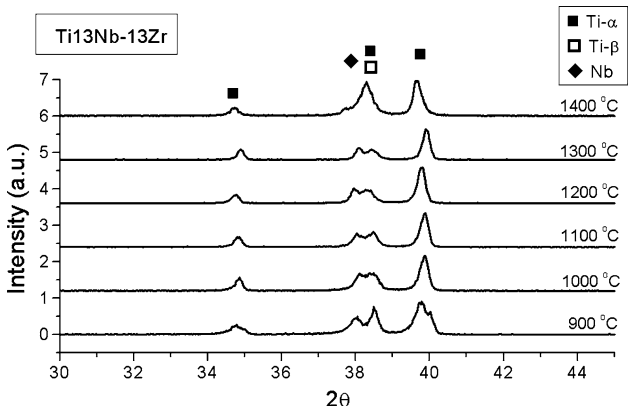

Fig. 5 XRD patterns showing the dissolution of niobium with increasing temperature and the subsequent formation of the Ti–13Nb–13Zr alloy

hydrides, oxides, or intermetallics (Fig. 5). The XRD analysis is difficult because the peaks of the beta stabilizers (Nb, in this case) and β-Ti-phase are almost the same. With an accurate analysis, the most noticeable feature is the reduction in the intensity of Nb peaks with increasing sintering temperature. The diffractions peaks corresponding of pure titanium and niobium were observed at 900 °C, since the alloying starts in this temperature, as showed by the microstructural analysis. In the temperature range between 900 and 1,300 °C, a continuous Nb dissolution, in both, α and β phases, is observed. Therefore, the analysis in 2θ range between 37° and 39° indicates the reduction of the Nb peaks intensity with increasing sintering temperature. The α and β peaks are coincident in $2\theta \cong 38.5°$. Nb particles tend to dissolve at higher sintering temperatures (as proved by the microstructural analysis), being probably absent in samples sintered above 1,400 °C. The total XRD pattern of the sample sintered at 1,400 °C is showed in Fig. 6, presenting only peaks from α and β Ti phases.

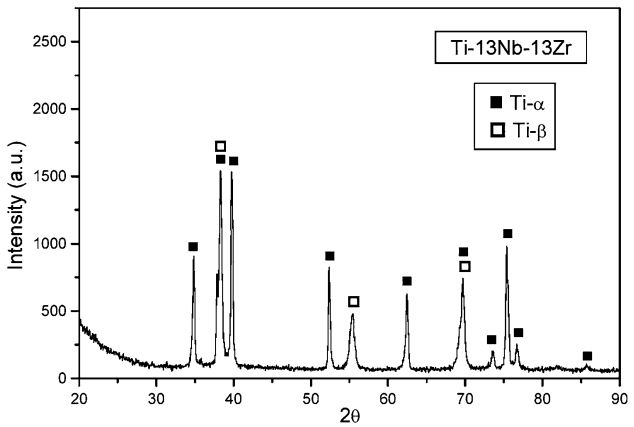

Fig. 6 XRD pattern of sample sintered at 1,400 °C/2 h

Dilatometric behavior

The expansion/contraction behavior during sintering of a Ti–13Nb–13Zr compact using hydrided and dehydrided powders were investigated by a dilatometer. The results are shown in Fig. 7. In the Ti–13Nb–13Zr sample produced from dehydrided powders, the compact expanded slightly as temperature increased. Contraction owing to densification started from about 900 °C. This temperature is close to the β transus temperature of titanium powders. Thus, the diffusivity of Nb and Zr in Ti matrix is activated through the range of temperatures at which titanium is β phase. Similar behavior has been also observed during heating of other titanium alloys compacts [31]. Densification continued up to 1,200 °C and overall contraction exceeding 6% was achieved. In the Ti–13Nb–13Zr sample produced with hydrided powders, after expansion, the contraction begins from 440 °C, close to the dehydriding temperature. Densification continued up to 1,200 °C and overall contraction exceeding 11% was achieved. The contraction starts in a low temperature when compared with others titanium alloys sintered from dehydrided powders [31]. This fact indicates the influence of hydrogen (H) atoms in the sintering mechanisms, providing a contraction even in low temperatures. The fact of the sintering to begin in lower temperature suggests the possibility of BE–Ti–13Nb–13Zr production in low temperatures (800–1,000 °C) with longer holding times.

Mechanical properties

Mechanical properties obtained by flexion tests of five levels of relative density in samples sintered at 1,400 °C are compared in Table 4. The results showed that the strength is dependent on density and the values are above

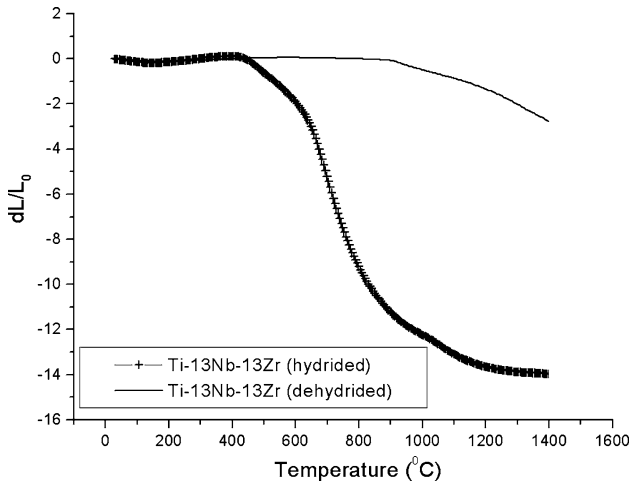

Fig. 7 Expansion/contraction behavior of a BE–Ti–13Nb–13Zr compact heated until 1,400 °C

Table 4 Mechanical properties obtained by flexion tests of five levels of relative density in samples sintered at 1,400 °C

Ti–13Nb–13Zr sample	Relative density	Ultimate strength (MPa)	*E* (GPa)	Elongation (%)
1	97.2	750	72.3	10.4
2	96.5	725	71.5	10.2
3	95.8	703	70.7	9.4
4	94.6	692	70.2	8.5
5	94.0	681	69.7	8.2

to the minimal requirements for orthopedic application [1]. The elastic modulus and the ductility increased remarkably with relative density for the studied samples. The dispersion of the densification values is due to the variation of Nb agglomeration after the samples blending that retard the sintering mechanism, reducing the densification. The elastic modulus is around 70 GPa, significantly lower than the metal alloys commonly used for surgical implants applications: Ti–6Al–4V (110 GPa), Ti–6Al–7Nb (105 GPa), stainless steel—316L (200 GPa), and cobalt-base alloys (200–230 GPa) [1].

Conclusion

Based on the isochronal sintering of BE–Ti–13Nb–13Zr samples, the following conclusions can be drawn: (a) The BE P/M process using hydrided powders can produce as-sintered high density titanium alloys; (b) Due to the complete dissolution of the alloy elements in the titanium matrix, a good combination of microstructure, mechanical properties and densification could be reached; (c) Nb plays an important role on microstructural development, however, Nb particles agglomeration must be avoided for a maximum densification; (d) The formation of two-phase areas ($\alpha + \beta$) begins at 900 °C with the dissolution of the smaller Nb particles. This structure grows with the dissolution of the Nb particles by the increase of the sintering temperature. A total homogeneous structure is only obtained after the complete dissolution of all the Nb particles; (e) The dilatometric analysis show that the alloy processing from hydrided powders is more efficient due to the acceleration of the sintering mechanisms; (f) The mechanical properties indicate that the strength is dependent on density; (g) The O pick-up is mainly related to the absorption during the hydriding and blending stages; and (h) The combination of relatively low-cost powders, compaction techniques in a mass production scale, vacuum sintering, minimal machining, and good mechanical properties can provide P/M Ti–13Nb–13Zr parts more attractive for surgical implants.

Acknowledgements The authors wish to thank to FAPESP—Fundação de Amparo à Pesquisa do Estado de São Paulo (proc.04/07664-2 and proc.08/04268-0), for the technician-scientific and financial support.

References

1. Long M, Rack HJ (1998) Biomaterials 19:1621
2. Niinomi M (2002) Metall Mater Trans A 33A:477
3. Ribeiro AA, Marques RFC, Guastaldi AC, Campos JSC (2009) J Mater Sci 44:4056. doi:10.1007/s10853-009-3585-6
4. Song Y, Xu DS, Yang R (1999) Mater Sci Eng A 260:269
5. Banerjee R, Nag S, Fraser HL (2005) Mater Sci Eng C 25:282
6. Ni YX, Feng B, Wang J, Lu X, Qu S, Weng J (2009) J Mater Sci 44:4031. doi:10.1007/s10853-009-3562-0
7. Nag S, Banerjee R, Fraser HL (2009) J Mater Sci 44:808. doi:10.1007/s10853-008-3148-2
8. Davidson JA, Kovacs P (1994) US Patent. 5.545.227
9. Bottino MC, Coelho PG, Yoshimot M, König B Jr, Henriques VAR, Bressiani AHA, Bressiani JC (2008) Mater Sci Eng C 28:223
10. Geetha M, Mudali UK, Gogia AK, Asokamani R, Raj B (2004) Corros Sci 46:877
11. Müller FA, Bottino MC, Müller L, Henriques VAR, Lohbauer U, Bressiani AH, Bressiani JC (2008) Dent Mater 24:50
12. Oliveira NTC, Ferreira EA, Duarte LT, Biaggio SR, Rocha Filho RC, Bocchi N (2006) Electrochim Acta 51:2068
13. Parga CJ, Varma SK (2009) Metall Mater Trans A 40:2987
14. Niemeyer TC, Grandini CR, Pinto LMC, Angelo ACD, Schneider SG (2009) J Alloys Compd 476:172
15. Duarte LT, Biaggio SR, Rocha Filho RC, Bocchi N (2009) J Mater Sci Mater Med 20:1009
16. Gutierrez A, Munuera C, Lopez MF, Jimenez JA, Morant C, Matzelle T, Kruse N, Ocal C (2006) Surf Sci 600:3780
17. Kretzer JP, Jakubowitz E, Krachler M, Thomsen M, Christian Heisel C (2009) Int Orthop 33:1531
18. Neikov OD, Naboychenko SS, Dowson G (2009) Handbook of non-ferrous metal powders. Elsevier Science, Oxford, UK
19. Henriques VAR, Sandim HRZ, Coelho GC, da Silva CRM (2003) Mater Sci Eng A 347:315
20. Taddei EB, Henriques VAR, Cairo CAA, Silva CRM (2004) Mater Sci Eng C 24:683
21. Henriques VAR, Galvani ET, Cairo CAA, Taddei EB (2008) Mater Sci Forum 591–593:24
22. Santos DR, Pereira MS, Cairo CAA, Graça MLA, Henriques VAR (2008) Mater Sci Eng A 472:193
23. Henriques VAR, Bellinati CE, Silva CRM (2001) J Mater Process Technol 118:212
24. Mao ZP, Ma J, Wang J, Sun B (2009) J Mater Sci 44:3265. doi:10.1007/s10853-009-3438-3
25. Senkov ON, Froes FH (1999) Int J Hydrogen Energy 24:565
26. Taddei EB, Henriques VAR, da Silva CRM, Cairo CAA (2007) Mater Res 10(3):289
27. Ueta MCC, Fracote CA, Henriques VAR, Graça MLA, Cairo CAA (2005) Mater Sci Forum 498–499:211
28. Li H, Yuan B, Gao Y, Chung CY, Zhu M (2009) J Mater Sci 44:875. doi:10.1007/s10853-008-3193-x
29. Boureau G, Capron N, Tétot R (2008) Scr Mater 59:1255
30. Donachie MJ (1988) Titanium: a technical guide. ASM, Metals Park
31. Fujita T, Ogawa A, Ouchi C, Tagima H (1999) Mater Sci Eng A 213:148